3D finite element modeling of water diffusion behavior of jute/PLA composite based on X-ray computed tomography

Ning Jiang[a,b*], Yaomin Li[a], Di Li[a*], Tao Yu[c], Yan Li[c], Jiachuan Xu[a], Ning Li[b], Thomas James Marrow[d]

a School of Transportation and Vehicle Engineering, Shandong University of Technology, Zibo 255049, PR China

b Research and Development Center, Triangle Tyre Co., Lid, Weihai 264200, PR China

c School of Aerospace Engineering and Applied Mechanics, Tongji University, 1239 Siping Road, Shanghai 200092, PR China

d Department of Materials, University of Oxford, Parks Road, Oxford OX1 3PH, United Kingdom

*Corresponding Authors:
Dr. Ning Jiang, E-mail: jiangning@sdut.edu.cn, Phone: +86-15221778806
Prof. Di Li, E-mail: hahali@sdut.edu.cn, Phone: +86-13573366162

Abstract: A three-dimensional (3D) finite element (FE) modeling approach, which includes the true internal microstructure of short plant fibre reinforced composites, is proposed to accurately simulate water diffusion behavior. The volume fraction, dimension and orientation distribution of jute fibres in a jute/PLA composite were acquired by segmentation of X-ray computed tomographs (XCT). Surface meshes of the jute fibre and PLA matrix were imported into Abaqus Finite Element (FE) software to establish a 3D model that was used to simulate water diffusion behavior at 23^{o} C. The ~~predicted~~ results were in good agreement with experimental measurements.

Keywords: A. Short-fibre composites; B. Hygrothermal effect; C. Finite element analysis (FEA); D. Non-destructive testing

1 Introduction

Plant fibre reinforced ploy (lactic acid) (PLA) composites have their excellent properties compared with conventional glass or aramid fibre reinforced composites[1-3], in particular recyclability, biodegradability and low density. The most promising applications of plant fibre/PLA composites are for lightweight components in aerospace and automobile applications, such as door trim, panels and seat due to their high specific strength and modulus. However, plant fibres are naturally hydrophilic and are quite susceptible to environmental factors such as external temperature and humidity, so their durability can be limited[4-6]. Anisotropy in the multi-scale microstructure and the distribution of plant fibres in composites can result in significant directionality in their water absorption behavior[7, 8], so to fully understand water diffusion behavior and the degradation mechanisms in plant fibre/PLA composites it is necessary to develop representative 3D model.

In recent years, a number of methods for generating solid models of fibre reinforced composites have been presented. In most studies, in order to reduce computational costs, the internal structures of the composites are directly built by random aggregate generation or with an assumed perfect periodicity of fibres that is obtained by experimental observations (i.e. SEM and visual examination). For unidirectional conventional synthetic fibres such as carbon or glass reinforced composites, many

works have focused on 2D models. For instance, Vaddadi et al.[7, 8] developed a numerical code to place circular fibres in random positions to establish a carbon/epoxy composite model with random fibre arrangements, and Joliff et al.[9] presented a 2D FE model (Abaqus) of a glass/epoxy composite, and used this to simulate water diffusion. Peret et al. [10] created the 2D FE model of glass fibre reinforced epoxy resin composites to analysis the water diffusion based on free volume theory. A random generator was used to create irregular geometries of the microstructure. Jain et al.[11] developed a 3D microstructure model by using FE Abaqus to study water diffusion both across and along the fibre length in a unidirectional fibre reinforced polymer matrix composites.

Different from the long traditional synthetic fibre reinforcement composite, the internal structure of short plant fibre reinforced PLA composites is complex and difficult to describe by approximate algebraic functions. So, it is important to observe and quantify the internal structure of a plant fibre/PLA composite in order to precisely establish a 3D FE model.

Various techniques have been used to investigate the internal structure of composites, such as the "tap test"[12], optical and fluorescence microscopy[13], acoustic emission[14, 15], ultrasonic[16], scanning electron microscopy (SEM)[17-19]. However, the non-imaging methods have limited resolution, and two-dimensional microscopy techniques also only provide limited information on the 3-dimensional structure, unless destructive sectioning is used. X-ray computed tomography (XCT) is a non-destructive

and high-resolution technique that can be used for 3D analysis of internal structures in composites. Many studies have now been conducted to demonstrate this utility. For instance, recently Jiang et al.[20] used XCT to evaluate the effects of hygrothermal degradation in jute/PLA composites, observing the development of material homogeneities, interface damage and microcracking. Saucedo-Mora et al.[21] used in situ XCT in SiC-SiC ceramic matrix composites to monitor the initiation and evolution of mechanical damage. Firas et al.[22] have also shown that XCT is useful in evaluate the density changes, reinforcement filler damage and microcracking caused by accelerated thermal degradation in epoxy resin composites.

Moreover, XCT allows 3D visualization and quantitative analysis of the microstructure. For instance, Zou et al.[23] employed high-resolution synchrotron XCT to characterize the crack distribution and porosity of fibre reinforced ceramic matrix composite, and Le and Garesci et al.[24, 25] showed how XCT could be used to quantify the fibre orientation and fibre volume content of composites. Such data provide a method to build models that are based on actual microstructures, and there are many examples of this in the literature. For instance, Sabiston et al.[26] established a Functionally Graded Interphase (FGI) model, using XCT-measured fibre orientation distributions, to predict the elastic response of long fibre sheet moulding compound composites. Straumit et al.[27] applied image processing methods (structure tensor) to XCT images to construct realistic models of woven carbon-epoxy composites. Iizuka et al.[28] established a 3D FE model with random fiber waviness for a unidirectional

carbon fibre reinforced plastic based on XCT images, and the compression was simulated. To date, the establishment of a 3D model of a short plant fibre reinforced composite based on XCT observations has not been reported.

In this paper, a 3D FE model of short jute fibre reinforced PLA composites is obtained from high resolution XCT observations. This model takes into account the material's true internal geometry, and the water diffusion behavior investigated with a finite element analysis that considers Fick's model. Finally, the simulation results are compared with the available experimental data.

2 Experimental

2.1 Materials

The Poly(lactic acid) (PLA) (4032*D*, molecular weight of 150,000 and a density of 1.25g/cm^3) was obtained from Suzhou Jiwang Environment Friendly Material Co. Ltd., China. The jute fibre yarn (3 strands twisted) was supplied by Shanghai Qiancong Jute Fibre Co. Ltd., China.

2.2 Specimens preparation

Injection moulding was used to prepare the jute/PLA composites. Firstly, the jute yarn and PLA granules were dried under vacuum at 60°C for 4h, and the fibres (diameter, 30–50μm) were cut to 2.5mm average length. Then the dried jute yarn and PLA were blended by using a SHJ-20 twin-screw extruder with 27mm screw diameter (feed rate=30g/min, screw speed=100rpm, length to diameter ratio (L/D)=40, Nanjing Jieya Co. Ltd., China). The weight fraction of jute fibre in the composite was 10%. The

jute/PLA composites were granulated using a YCT-132 granulator (Nanjing Jieya Co. Ltd., China), and dried under vacuum at 60°C for 4h. Finally, the test specimens of pure PLA and jute/PLA composite were produced respectively in a PL550/150 injection moulding machine (Wuxi Haitian Machinery Co. Ltd., China) with a barrel temperature of 175~180°C at an injection pressure of 55 Bar.

2.3 X-ray computed tomography (XCT)

XCT tomographs of the fibre/PLA composite were obtained with an X-ray microscope (Xradia Versa 510, Zeiss, Germany), operated at a voltage of 80kV and power of 7W to provide 3D X-ray attenuation images at a voxel size of 3μm. The cuboid specimen size was $4\times 6\times 4 mm^3$, obtained by cutting the center of an untested tensile specimen (Figure 1a). The scanned region (a cylinder with height 3mm and diameter 3mm) is shown in Figure 1b and example observations are shown in Figure 1c. A more detailed description of the XCT observations is given in a previous article[20].

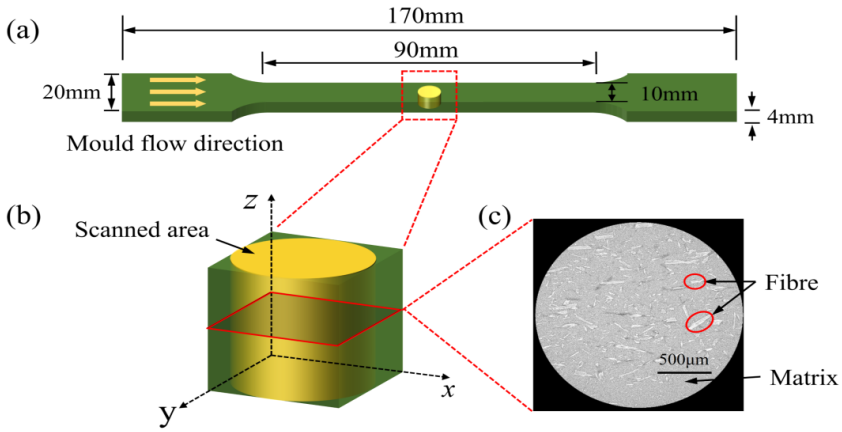

Figure 1: *Geometry of tensile specimens and the geometry used for the X-ray computed tomography: (a) Tensile specimen, (b) Scanned specimen and (c) XCT image. The mould flow direction is along the X-direction.*

2.4 Water absorption tests

Water absorption tests of the jute/PLA composite were in accordance with ASTM D5229[29], and the water absorption of pure PLA plastic was tested in accordance with ASTM D570-98[30]. The specimens ($30\times20\times4mm^3$) were dried in vacuum at 60°C for 24h before testing, and their initial weight (W_0) was then measured using a high precision balance (precision=$10^{-4}g$, Precisa-XR, Switzerland). The specimens were immersed into deionized water baths at 23°C. The Weight (W_t) was recorded at each periodic removal of the specimen until saturation, and the weight gain (%) (M_t) was calculated with Eq. (1).

$$M_t = \frac{W_t - W_0}{W_0} \times 100\% \tag{1}$$

Five specimens were tested to obtain the average and standard deviation. The weight gain of jute fibres was then estimated, using the measured weight gain for the pure PLA sample at the same time interval, by use of a scale model[31, 32], as Eq. (2).

$$\Delta W_{jute/PLA} = \Delta W_{jute} \times V_{jute} + \Delta W_{PLA} \times (1 - V_{jute}) \tag{2}$$

Where $\Delta W_{jute/PLA}$, ΔW_{jute} and ΔW_{PLA} are the weight gain of jute/PLA composite, jute fibres and PLA, respectively. V_{jute} is the volume content of jute fibres (8.5%, measured by XCT).

3 Results and discussion

3.1 3D FE model establishment

3.1.1 Threshold segmentation and quantitative analysis

Quantitative analysis and 3D reconstruction of the tomography images by threshold segmentation were done by using the Avizo 9.0 software (Visualization Sciences Group,

Bordeaux, France). The detailed operation process is summarized in Figure 2. A 3D dimensional view of the raw data in shown in Figure 3a. Before segmentation, 3D median filtering was applied to reduce the image noise (Figure 3b), and the data was cropped to a region of interest (ROI) of $2\times2\times2mm^3$. Each voxel of the 3D dataset measures a grey level that depends on the relative X-ray attenuation coefficient of the material within it. Figure 3c, d shows greyscale orthogonal views of the jute/PLA composites. Good image contrast has been obtained between the features of the microstructure, so the jute fibre and PLA matrix can be clearly distinguished.

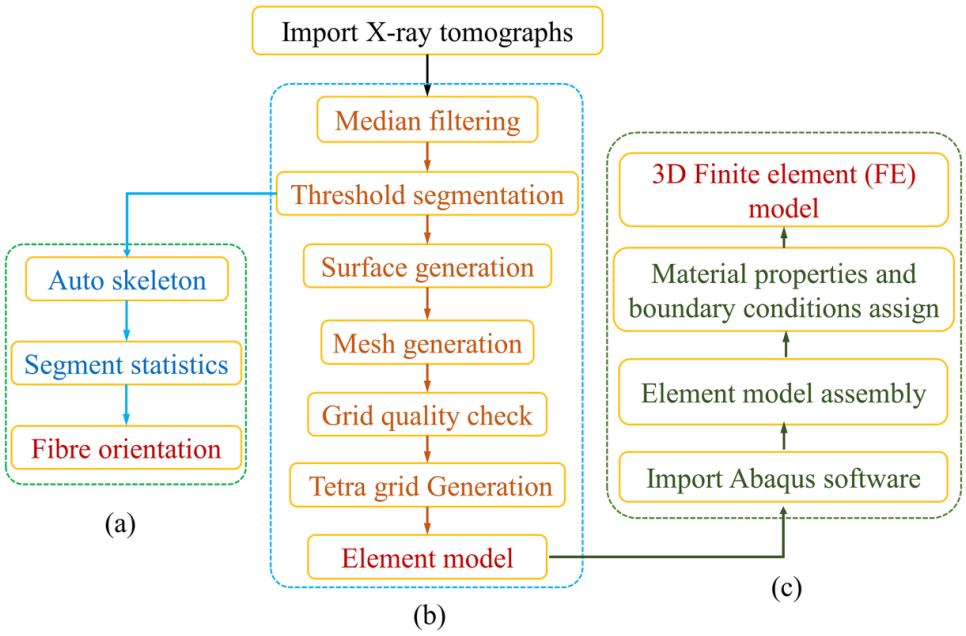

Figure 2: *Quantitative analysis and process of 3D FE model establishment: (a) orientation distribution analysis of jute fibre, (b) 3D model reconstruction and (c) 3D FE model generation.*

To segment the tomography data, grey level thresholds to separate the different phases must be chosen. The grey level histograms (Figure 3e), shows that threshold ranges (as 8bit data) can be chosen as 0-131, 131-189, 189-255 to separate the porosity,

matrix and fibres respectively by segmentation. Some islands occurred in the segmentation by thresholding of fibre (Figure 3f). These islands with length below 30μm (diameter of jute fibre was 30–50μm) may caused by the data noise and were removed (Figure 3g) by dimensional analysis function. The analysis of the volume content of jute fibre was determined to be 8.5%, which is consistent with the fibre weight fraction (10%) from manufacture. This proves the accuracy of the extracted fibre.

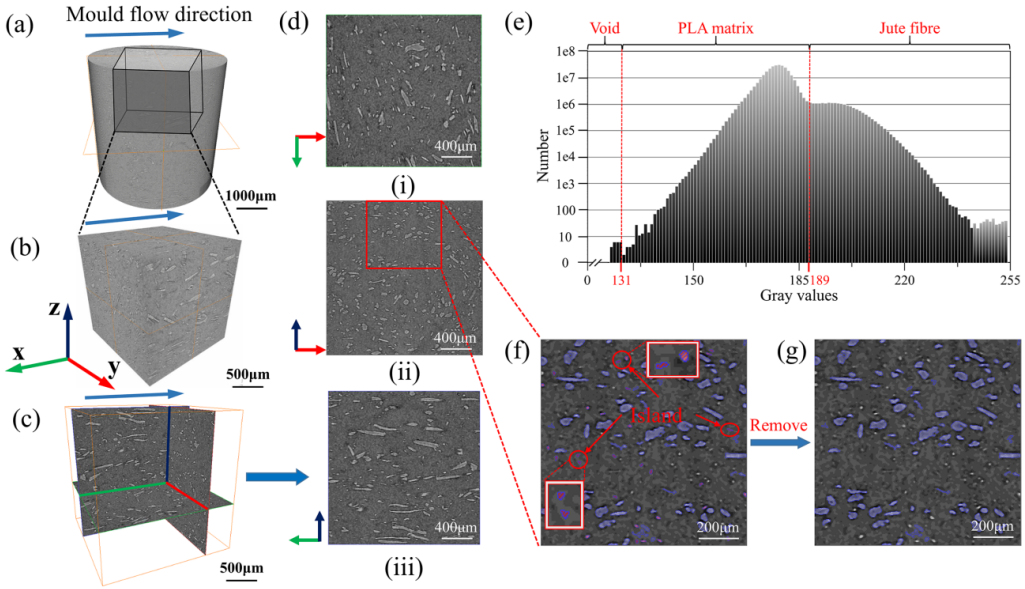

Figure 3: *Threshold segmentation of jute/PLA composite: (a) 3D dimensional view, (b) region of interest, (c) and (d) show ortho view images of the jute/PLA composites, (e) number of voxels per grey value, (f) segmentation of fibers from the matrix by applying threshold, (g) island removal.*

By inspection, the jute fibres appear to be oriented in the mould flow direction (i.e. X direction defined in Figure 1). To verify this, the skeletonization algorithm of the Avizo software is used for a quantitative analysis of the orientations of the Euler polar coordinates of the fibres that had been identified by segmentation of the tomography data (Figure 4). This shows that the polar angle (θ) of 75% jute fibre inside the

composite is concentrated within 20° in the XY plane (Figure 4b), and nearly 71% of the jute fibres have their azimuth angle (φ) within 40° of X direction (Figure 4c). This preferential alignment is due to the high shear stress of the material flow in the mould flow direction during the moulding process. This anisotropy may be expected to affect the directionality of the water absorption behavior, and is an important reason for the establishment of real FE model to simulation analysis.

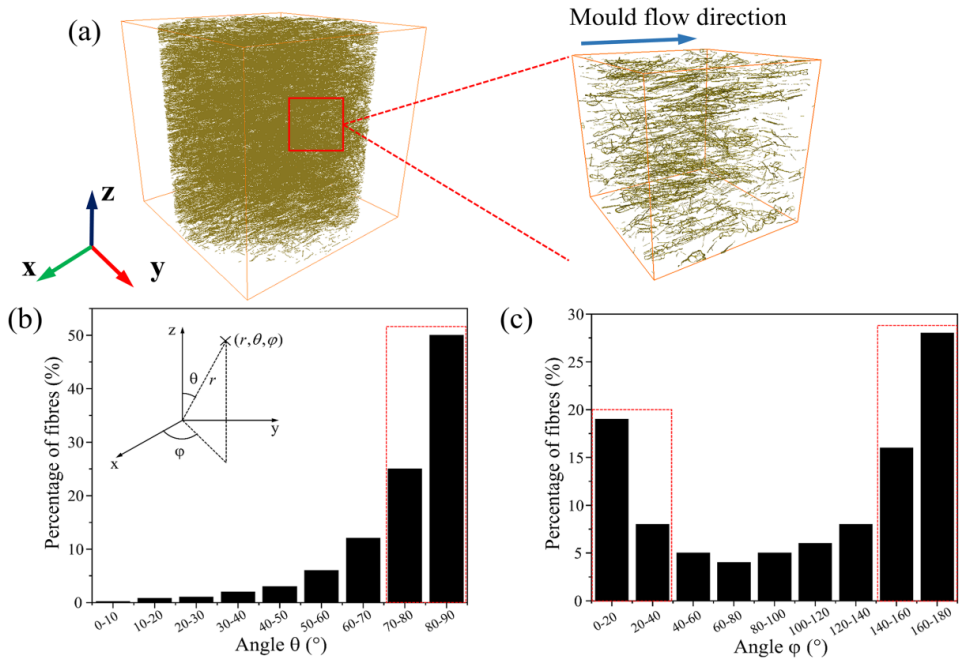

Figure 4: *Analysis of orientation distribution of jute fibre: (a) jute fibre skeletonization. The orientation distributions of the fibres (Euler polar coordinates) are summarized in (b) polar angle, θ; and (c) azimuthal angle, φ.*

3.1.2 3D reconstruction and FE model

The small amount of porosity (0.05%) was neglected, and the composite is considered as a two-phase material of fibre and matrix. Figure 5a, b (i) shows a 3D volume rendering of the segmented jute fibres. In order to construct a 3D mesh composed of 3D elements or cells, it is necessary to construct a 3D surface of each

volume boundary. After threshold segmentation, a surface was obtained by a smoothing function, as shown in Figure 5b (ii). Then, the jute fibre is meshed to generate a tetrahedral mesh, with a mesh size of 0.05-0.1*mm* (Figure 5b (iii)). At last, the element model of jute fibre after 3D reconstruction is established in Figure 5c. The PLA matrix were reconstructed by the same method.

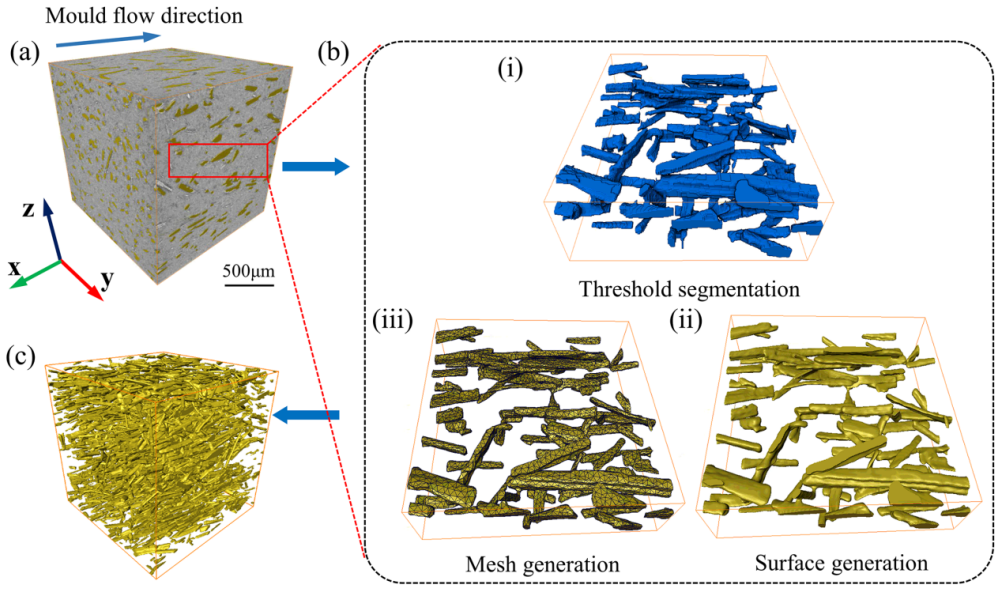

Figure 5: *Process of 3D reconstruction of jute fibre: (a) 3D volume rendering of segmented jute fibre, (b) 3D surface reconstruction process and (c) jute fibre element model.*

The 3D volume rendering of the segmented PLA matrix is shown in Figure 6a. After applying surface building and mesh functions (Figure 6b), some mesh defects (i.e. sharp corners, intersections, chamfers, coplanarities, coincident edges) was observed in the PLA matrix (Figure 6c), or in the jute fibres, demonstrating locally low mesh quality. The Avizo command operation of 'recompute connectivity' was applied to remove these mesh error, and obtain a higher quality tetrahedron grid. Finally, the establishment of the 3D element model of PLA matrix was completed, as shown in Figure 6d.

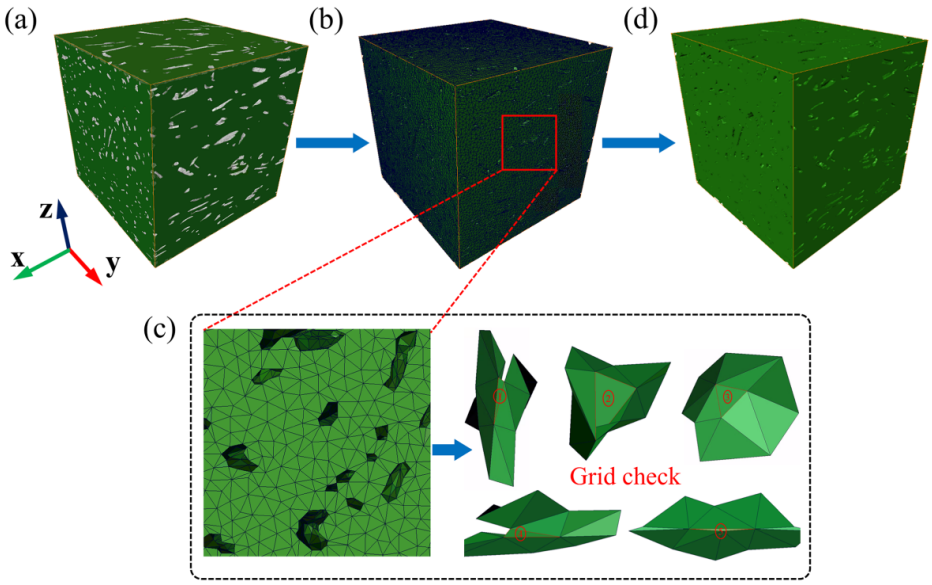

Figure 6: *Process of 3D reconstruction of PLA matrix: (a) 3D volume rendering of segmented PLA matrix, (b) surface and mesh generation, (c) grid quality check and (d) PLA matrix element model.*

The full process of 3D FE model establishment of jute/PLA composite is summarized in Figure 2c and Figure 7. After threshold segmentation (Figure 7a, b), the 3D reconstruction element model of jute fibres and PLA matrix (Figure 7c) was completed after surface and mesh generation in the Avizo 9.0 software. There are 424054 and 2892552 tetrahedral elements for jute fibre and PLA matrix, correspondingly. Then, the element model of the jute fibre and PLA matrix was exported into the Abaqus FE software, as shown in Figure 7d. After the assembly of fibre and matrix, and assignment of material parameters and boundary conditions in Abaqus, the 3D FE model of jute/PLA composites was established in Figure 7e.

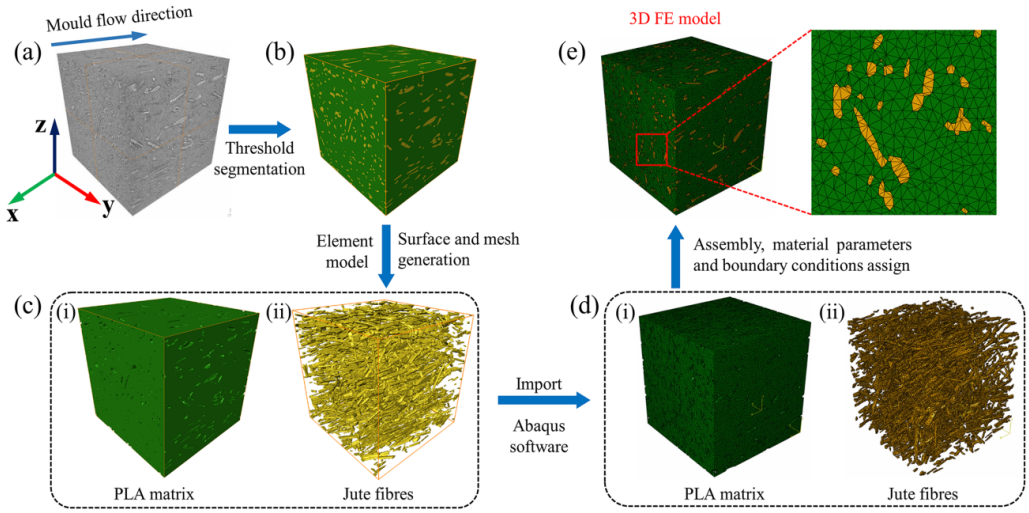

Figure 7: *Process of 3D FE model establishment: (a) 3D dimensional view, (b) 3D volume rendering by applying a threshold segmentation, (c) 3D reconstruction element model of jute fibre and PLA matrix after surface and mesh generation, (d) element model of jute fibre and PLA matrix in Abaqus software, (e) 3D FE model is built with the assembly of jute fibre and PLA matrix, material parameters and boundary conditions.*

3.2 Water diffusion behavior

The measured M_t for pure PLA and jute/PLA composites at different time under 23^o C is shown in Figure 8a. The M_t of jute fibres was estimated by Eq. (2). The saturated mass gain, M_m, is 25.80% for the jute fibres, which is significantly higher than that of jute/PLA composite (2.80%) and pure PLA (0.65%). This can be explained by the fact that the plant fibre structure contains a large number of hydroxyls of cellulose and lumens, which promote the transportation[33] and storage of water[34]. In order to describe the water absorption behavior of jute/PLA composite, weight gain curves determined by Eq. (3)[35] were fitted (Figure 8b)

$$\frac{M_t}{M_m} = kt^n \tag{3}$$

Where k, n represents the diffusion kinetic parameters.

The fit shows the values of n are all close to 0.5, demonstrating that the water diffusion of pure PLA, jute fibre and jute/PLA composites can be approximated by Fick's law. Therefore, for values M_t/M_m lower than ~0.6, the initial part of the weight gain curve can be expressed by Eq. (4)[36] :

$$\frac{M_t}{M_m} = \frac{4}{h}\left(\frac{D}{\pi}\right)^{1/2} \cdot t^{1/2} \tag{4}$$

Where h is the thickness of the specimen and D is the diffusion coefficient.

For M_t/M_m higher than 0.6, the absorption curve approximates Eq. (5)[36]:

$$\frac{M_t}{M_m} = 1 - exp\left[-7.3\left(\frac{D \cdot t}{h^2}\right)^{0.75}\right] \tag{5}$$

The diffusion coefficient D, determined from Eq. (4), can usually be expressed as Eq. (6) [35]:

$$D = \frac{\pi}{(4M_m)^2} \times \left(\frac{M_t \times h}{\sqrt{t}}\right)^2 = \frac{\pi k'^2}{(4M_m)^2} \tag{6}$$

Where the coefficient k' is the slope of the linear part of the curve $M_t = f(\sqrt{t}/h)$.

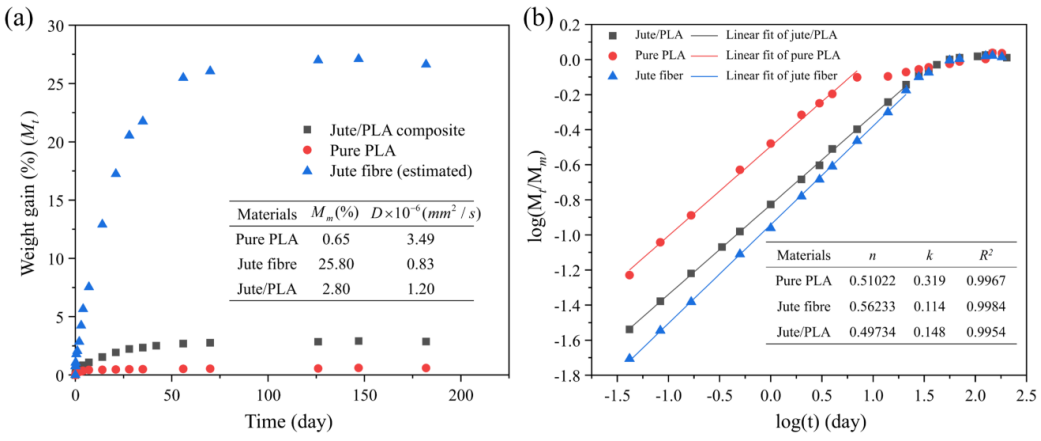

Figure 8: *Determination of water absorption kinetic parameters: (a) weight gain (M_t) of jute/PLA composite, pure PLA and jute fibre (estimated), (b) Diffusion curve fitting plots of jute/PLA composites, pure PLA and jute fibre.*

The obtained diffusion coefficients of pure PLA ($3.49\times 10^{-6} mm^2/s$) and jute/PLA composites ($1.20\times 10^{-6} mm^2/s$) are listed in Figure 8a Although the M_t of jute/PLA composite is higher than pure PLA, the value of D for jute/PLA composite was smaller than pure PLA. This can be explained by the fact that the addition of jute fibre not only promoted the water absorption but also increased the value of M_m[37], resulting in a prolonged saturation time of the fibre, thus leading to a lower overall D value.

The M_m and D of PLA resin and jute fibre are required to model the water diffusion behavior of jute/PLA composites. The water diffusion behavior of pure PLA resin is assumed isotropic, where $D=3.49\times 10^{-6} mm^2/s$. For the jute fibre, its multi-scale structure makes its diffusion behavior anisotropic, and its longitudinal and transverse diffusion coefficients need to be determined separately[38, 39]. However, in this work, the water diffusion principally occurs across the thickness of the jute/PLA composites which is in the transverse direction of major jute fibres. Hence, only the transverse diffusion coefficient of the jute fibre is considered, and the longitudinal diffusion coefficient of the jute fibre is ignored to simplify the estimation of the diffusion coefficient. Therefore, based on the jute fibre weight gain curve obtained by Eq. (2), the estimated value of the diffusion coefficient for the jute fibres in this composite was $0.83\times 10^{-6} mm^2/s$. This is close to the value for jute fibres ($D_f=1.12\times 10^{-6} mm^2/s$), measured in isolation, that is reported in the literature[40].

3.3 Finite element simulation

The water diffusion behavior of jute/PLA composites was simulated by Abaqus mass

diffusion analysis, using four-node linear heat transfer tetrahedral elements DC3D4. The dimension of half-thickness model, water boundary conditions and diffusion parameters of jute fibre and PLA matrix are illustrated in Figure 9. The arithmetic mean of the water concentrations of all nodes in the jute/PLA model was taken as the M_t.

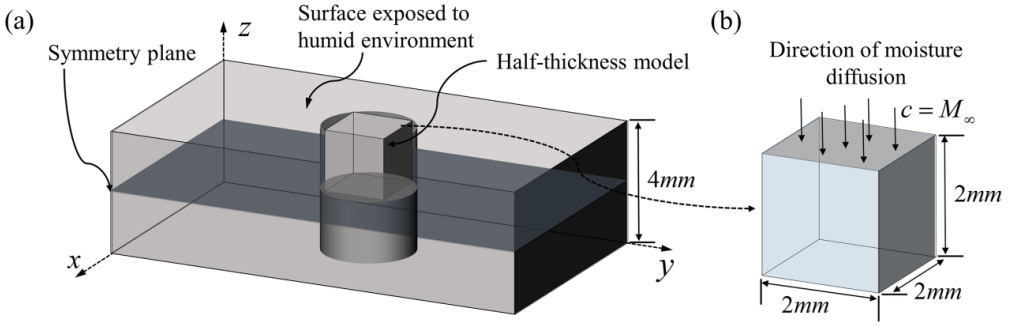

(c) Diffusion parameters of jute fibre and PLA matrix

Materials	M_m(%)	$D \times 10^{-6} (mm^2/s)$
PLA matrix	0.65	3.49
Jute fibre	25.80	0.83

Figure 9:*Boundary conditions of the 3D FE model of jute/PLA composites specimen: (a) thin composite specimen is exposed to humid environment at up and down surfaces, (b) The half-thickness model that is used in the analysis, (c) diffusion parameters of jute fibre and PLA matrix.*

The FE results obtained with the values of jute fibre and PLA matrix in Figure 9c are shown in Figure 10. The results show that the geometric model with the *D* value of 0.83 $\times 10^{-6} mm^2/s$ for jute fibre not correctly fit the experimental water absorption curve. A good fit was obtained by significantly increasing the diffusion coefficient of the jute fibre to D=0.97$\times$ $10^{-5} mm^2/s$. This indicates that the jute fibre present the different diffusion behavior when they are taken separately and mixed into the composites. This tendency has been already observed in flax/epoxy composite[41]. According to Chilali et al.[41], it can be explained by the fact that volume of flax fibre is reduced due to the

confine of epoxy resin. This could explain the difference diffusion coefficient when it is confined in the matrix and when it is aged solely.

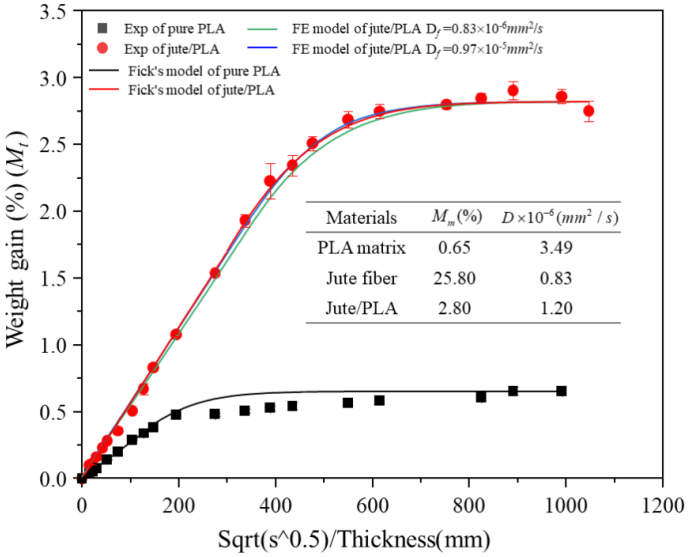

Materials	M_m(%)	$D\times10^{-6}$(mm^2 / s)
PLA matrix	0.65	3.49
Jute fiber	25.80	0.83
Jute/PLA	2.80	1.20

Figure 10: *Comparison between the experimental data, Fick's model and FE models of weight gain curves of jute/PLA composites using D_f=0.83×10^{-6}mm^2/s and D_f=0.97×10^{-5}mm^2/s.*

Through the water diffusion behavior simulation of 3D EF model of jute/PLA composites, the evolutions of transient water diffusion is studied. Figure 11 illustrates the water distribution with in the jute/PLA composite (Figure 11a), jute fibres (Figure 11b) and PLA matrix (Figure 11a) for four different time of 24, 90, 720 and 2160 hrs. At the region near the surface where directly contact with water, the moisture content immediately reaches M_m of PLA matrix (Figure 11b) and jute fibres (Figure 11c). Subsequently, the water diffuses toward the symmetric center plane as time increased. It can be seen that the water does not diffuse completely uniformly across the thickness (XY plane) of PLA matrix and jute fibres in the early time plots (t= 24, 90 and 720h). This occurs due to the clustering of short jute fibres. Since most of water diffuse through the jute fibres in the composite, local aggregation of jute fibres can promote the

water absorption process in the corresponding area. In addition, the orientation and the anisotropy diffusion coefficient of jute fibre also contribute to this phenomenon. In the first 720h, the water diffusion is very fast, the jute/PLA composites almost saturated at 720h except near the symmetry plane. Thereafter, fully saturation is not reached until 2160h. At later time, the composite absorbs a limited amount of moisture, so only a small additional weight gain can be obtained. The result is consistent with the water absorption test which proved the correctness of 3D FE model.

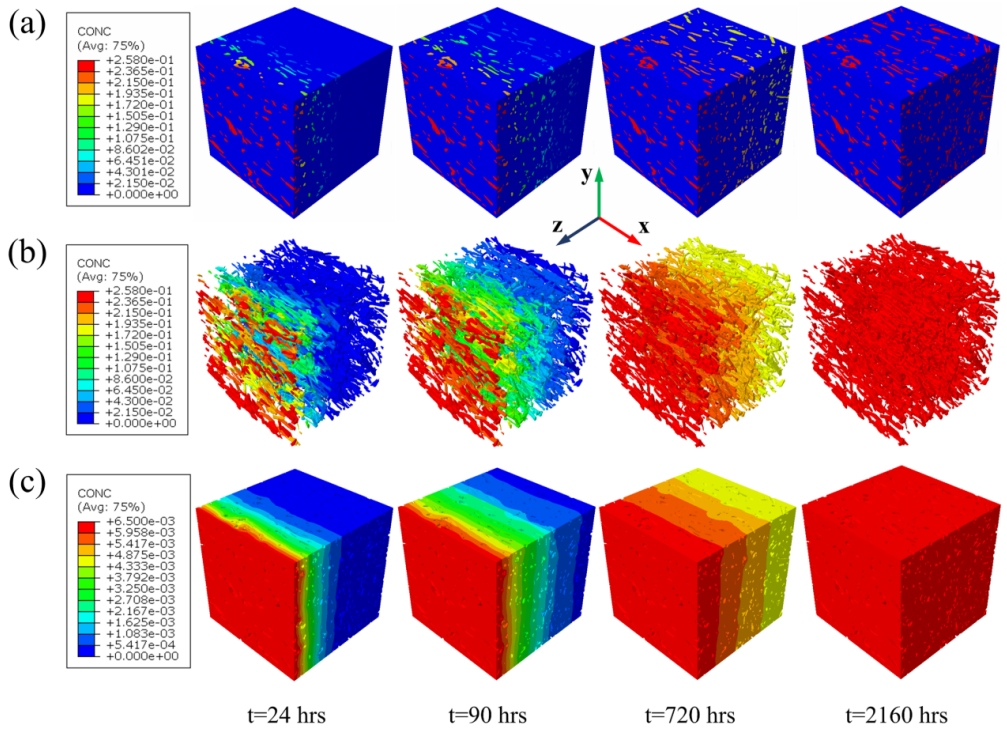

Figure 11: *Transient moisture distribution within (a) jute/PLA composite, (b) jute fibre and (c) PLA matrix are shown at four different times.*

4 Conclusion

XCT is successfully used to characterize the internal microstructure of short jute fibre reinforced PLA composite. The threshold-based segmentation procedure is able to

separate the jute fibre and PLA matrix and visualize directly the internal structure of jute/PLA composites. The volume content of jute fibre was determined to be 8.5% and most jute fibres aligned with the mould flow direction due to the high shear in the flow direction during moulding after quantitative analysis of the tomography data.

3D FE model was established in four steps: (i) threshold segmentation, (ii) 3D surface reconstruction of jute fibre and PLA matrix, (iii) establishing of element model of the jute fibre and PLA matrix with mesh generation, (iv) assembly of element model in Abaqus, and assign of related material parameters and boundary conditions. Then the 3D FE model have been used to simulation the water diffusion behavior of jute/PLA composites in 23^{o} C by using Abaqus software. The water absorption behavior of the jute/PLA composite is simulated, and the diffusion process of water in the material can be observed intuitively. The numerical investigation of the water diffusion behavior of the jute/PLA specimens permitted an estimation of the jute fibre transverse diffusion coefficient, which quite different from estimated with simple Fickian analysis of the experimental results. This indicates that the jute fibre diffusion behavior is modified when confined in the PLA resin. The simulation also predicts that water does not diffuse completely uniformly due to the clustering of short jute fibres.

The model described in this paper have helped to understand the water diffusion behavior and mechanisms of jute/PLA composites in the hygrothermal environment. The multi-scale modelling approach developed can be applied to a selection of samples of microstructure to extract the properties of moisture diffusion of composite.

Acknowledgements

This work is supported by the Scientific Research Foundation of Shandong University of Technology (No. 4041/419002). EPSRC Grant EP/M02833X/1 "University of Oxford: experimental equipment upgrade" supported the Xradia Versa 510 microscope and facilities for data analysis and visualization.

References

[1] A. Sangregorio, N. Guigo, J.C. van der Waal, N. Sbirrazzuoli, All 'green'composites comprising flax fibres and humins' resins, Compos. Sci. Technol., 171 (2019), pp. 70-77.
[2] K.L. Pickering, M.A. Efendy, T.M. Le, A review of recent developments in natural fibre composites and their mechanical performance, Compos. Part A Appl. Sci. Manuf., 83 (2016), pp. 98-112.
[3] M.P. Ho, H. Wang, J.H. Lee, C.K. Ho, K.T. Lau, J. Leng, D. Hui, Critical factors on manufacturing processes of natural fibre composites, Compos. B Eng., 43 (2012), pp. 3549-3562.
[4] J.C. Halpin, Effects of environmental factors on composite materials, Air Force Materials Lab Wright-Patterson AFB OH, 1969.
[5] L.Y. Mwaikambo, M.P. Ansell, Chemical modification of hemp, sisal, jute, and kapok fibers by alkalization, J. Appl. Polym. Sci., 84 (2002), pp. 2222-2234.
[6] H. Dhakal, Z. Zhang, M. Richardson, Effect of water absorption on the mechanical properties of hemp fibre reinforced unsaturated polyester composites, Compos. Sci. Technol., 67 (2007), pp. 1674-1683.
[7] P. Vaddadi, T. Nakamura, R.P. Singh, Transient hygrothermal stresses in fiber reinforced composites: a heterogeneous characterization approach, Compos. Part A Appl. Sci. Manuf., 34 (2003), pp. 719-730.
[8] P. Vaddadi, T. Nakamura, R.P. Singh, Inverse analysis for transient moisture diffusion through fiber-reinforced composites, Acta Mater., 51 (2003), pp. 177-193.
[9] Y. Joliff, L. Bélec, J.F. Chailan, Modified water diffusion kinetics in an unidirectional glass/fibre composite due to the interphase area: Experimental, analytical and numerical approach, Compos. Struct., 97 (2013), pp. 296-303.
[10] T. Peret, A. Clement, S. Freour, F. Jacquemin, Effect of mechanical states on water diffusion based on the free volume theory: Numerical study of polymers and laminates used in marine application, Compos. B Eng., 118 (2017), pp. 54-66.
[11] D. Jain, A. Mukherjee, Three-dimensional hygromechanical analysis of fibre polymer composites: Effect of boundary conditions, Compos. B Eng., 90 (2016), pp. 203-211.
[12] D.K. Hsu, D.J. Barnard, J.J. Peters, V. Dayal, Physical basis of tap test as a quantitative imaging tool for composite structures on aircraft, In: Proceedings of AIP Conference, (2000), p.1857-1864.
[13] R. Young, Analysis of composites using raman and fluorescence microscopy—a review, J. Microc. Oxford, 185 (1997), pp. 199-205.
[14] F.E. Oz, S. Ahmadvashaghbash, N. Ersoy, Damage mode identification in transverse crack tension specimens using acoustic emission and correlation with finite element progressive damage model, Compos. B Eng., 165 (2019), pp. 84-95.

[15] M. Saeedifar, M.A. Najafabadi, D. Zarouchas, H.H. Toudeshky, M. Jalalvand, Barely visible impact damage assessment in laminated composites using acoustic emission, Compos. B Eng., 152 (2018), pp. 180-192.
[16] V.K. Kinra, A.S. Ganpatye, K. Maslov, Ultrasonic ply-by-ply detection of matrix cracks in laminated composites, J. Nondestruct. Eval., 25 (2006), pp. 37-49.
[17] N. Jiang, T. Yu, Y. Li, Effect of hydrothermal aging on injection molded short jute fiber reinforced poly (lactic acid)(PLA) composites, J. Polym. Environ., 26 (2018), pp. 3176-3186.
[18] M. Cai, H. Takagi, A.N. Nakagaito, Y. Li, Waterhouse GI, Effect of alkali treatment on interfacial bonding in abaca fiber-reinforced composites, Compos. Part A Appl. Sci. Manuf., 90 (2016), pp. 589-597.
[19] W.J. Lee, A.J. Clancy, E. Kontturi, A. Bismarck, M.S. Shaffer, Strong and stiff: high-performance cellulose nanocrystal/poly(vinyl alcohol) composite fibers, ACS Appl. Mater. Inter., 8 (2016), pp. 31500-31504.
[20] N. Jiang, T. Yu, Y. Li, T.J. Pirzada, T.J. Marrow, Hygrothermal aging and structural damage of a jute/poly (lactic acid)(PLA) composite observed by X-ray tomography, Compos. Sci. Technol., 173 (2019), pp. 15-23.
[21] L. Saucedo-Mora, T. Lowe, S. Zhao, P.D. Lee, P.M. Mummery, T.J. Marrow, In situ observation of mechanical damage within a SiC-SiC ceramic matrix composite, J. Nucl. Mater., 481 (2016), pp. 13-23.
[22] F. Awaja, B. Arhatari, K. Wiesauer, E. Leiss, D. Stifter, An investigation of the accelerated thermal degradation of different epoxy resin composites using X-ray microcomputed tomography and optical coherence tomography, Polym. Degrad. Stab., 94 (2009), pp. 1814-1824.
[23] C. Zou, T.J. Marrow, C. Reinhard, B. Li, C. Zhang, S. Wang, Porosity characterization of fiber-reinforced ceramic matrix composite using synchrotron X-ray computed tomography, J. Instrum., 11 (2016), C03052.
[24] T.H. Le, P.J. Dumont, L. Orgéas, D. Favier, L. Salvo, E. Boller, X-ray phase contrast microtomography for the analysis of the fibrous microstructure of SMC composites, Compos. Part A Appl. Sci. Manuf., 39 (2008), pp. 91-103.
[25] F. Garesci, S. Fliegener, Young's modulus prediction of long fiber reinforced thermoplastics, Compos. Sci. Technol., 85 (2013), pp. 142-147.
[26] T. Sabiston, P. Pinter, J. Lévesque, K.A. Weidenmann, K. Inal, Evaluating the number of fibre orientations required in homogenization schemes to predict the elastic response of long fibre sheet moulding compound composites from X-ray computed tomography measured fibre orientation distributions, Compos. Part A Appl. Sci. Manuf., 114 (2018), pp. 278-294.
[27] I. Straumit, S.V. Lomov, M.Wevers, Quantification of the internal structure and automatic generation of voxel models of textile composites from X-ray computed tomography data, Compos. Part A Appl. Sci. Manuf., 69 (2015), pp. 150-158.
[28] K. Iizuka, M. Ueda, T. Takahashi, A. Yoshimura, M. Nakayama, Development of a three-dimensional finite element model for a unidirectional carbon fiber reinforced plastic based on X-ray computed tomography images and the numerical simulation on compression, Adv. Compos. Mater., 28 (2019), pp. 73-85.
[29] ASTM D5229/D5229M-14. Standard test method for moisture absorption properties and equilibrium conditioning of polymer matrix composite materials, West Conshohocken, PA: ASTM International, 2014.
[30] ASTM D570-98. Standard test method for water absorption of plastics, West Conshohocken, PA:

ASTM, 2010.
[31] J.H. Affdl, J. Kardos, The Halpin-Tsai equations: a review, Polym. Eng. Sci., 16 (1976), pp. 344-352.
[32] A. Le Duigou, A. Bourmaud, P. Davies, C. Baley, Long term immersion in natural seawater of Flax/PLA biocomposite, Ocean Eng., 90 (2014), pp. 140-148.
[33] K. Oksman, M. Skrifvars, J.F. Selin, Natural fibres as reinforcement in polylactic acid (PLA) composites, Compos. Sci. Technol., 63 (2003), pp. 1317-1324.
[34] M. Kabir, H. Wang, K. Lau, F. Cardona, Chemical treatments on plant-based natural fibre reinforced polymer composites: An overview, Compos. B Eng., 43 (2012), pp. 2883-2892.
[35] M. Assarar, D. Scida, A. El Mahi, C. Poilâne, R. Ayad, Influence of water ageing on mechanical properties and damage events of two reinforced composite materials: Flax–fibres and glass–fibres, Mate. Des., 32 (2011), pp. 788-795.
[36] C.H. Shen, G.S. Springer, Moisture absorption and desorption of composite materials, J. Compos. Mater., 10 (1976), pp. 2-20.
[37] B. Madsen, Properties of plant fiber yarn polymer composites: an experimental study, Technical University of Denmark (DTU), 2004.
[38] C. Baley, Analysis of the flax fibres tensile behaviour and analysis of the tensile stiffness increase, Compos. Part A Appl. Sci. Manuf., 33 (2002), pp. 939-948.
[39] A. Zykwinska, J.F. Thibault, M.C. Ralet, Competitive binding of pectin and xyloglucan with primary cell wall cellulose, Carbohydr. polym., 74 (2008), pp. 957-961.
[40] A. Célino, S. Fréour, F. Jacquemin, P. Casari, Characterization and modeling of the moisture diffusion behavior of natural fibers, J. Appl. Polym. Sci., 130 (2013), pp. 130(1)297-306.
[41] A. Chilali, M. Assarar, W. Zouari, H. Kebir, R. Ayad, Analysis of the hydro-mechanical behaviour of flax fibre-reinforced composites: Assessment of hygroscopic expansion and its impact on internal stress, Compos. Struct., 206 (2018), pp. 177-184.

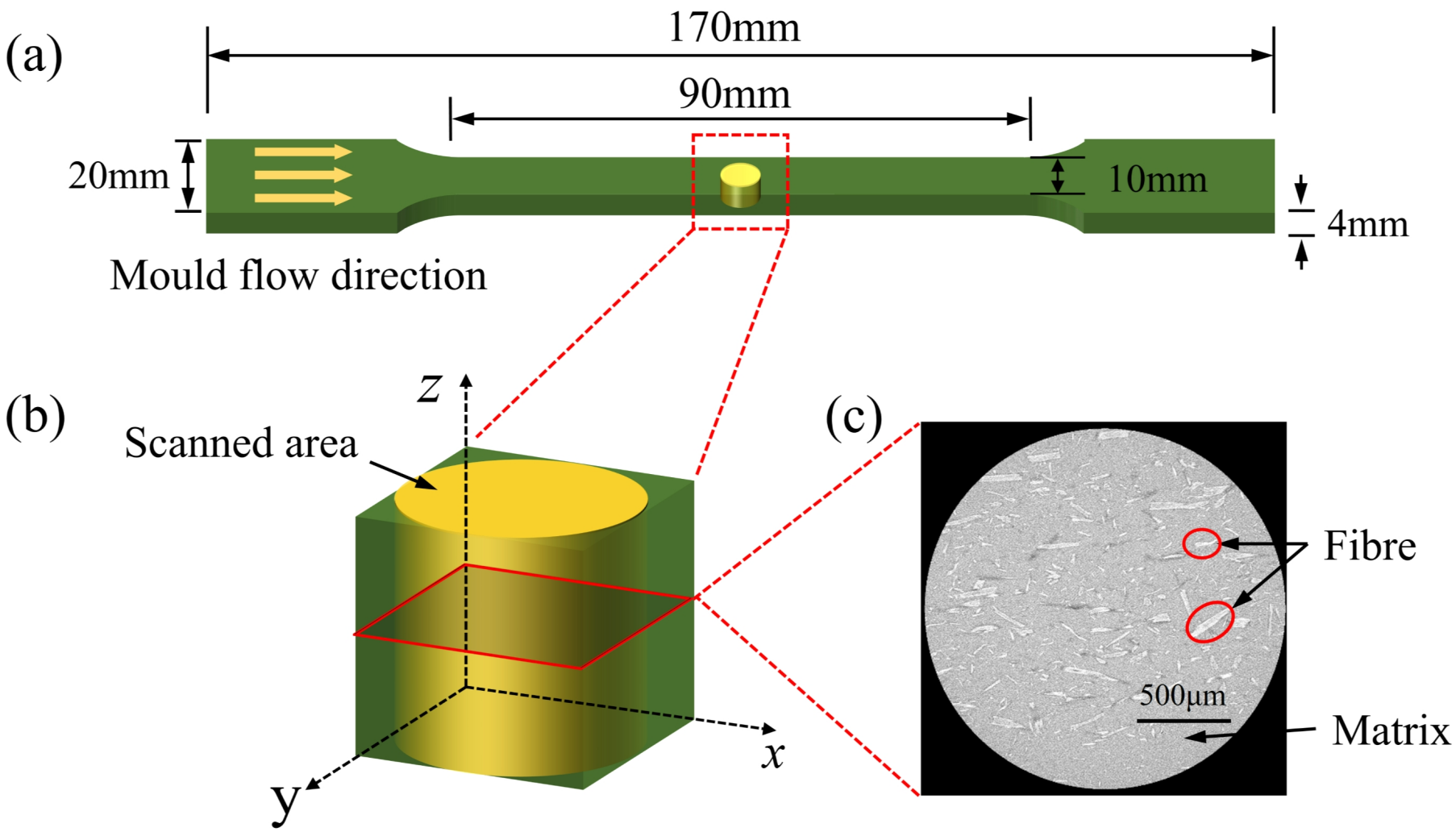
(a)
170mm
90mm
20mm
10mm
4mm
Mould flow direction
(b)
Scanned area
z
x
y
(c)
Fibre
500μm
Matrix

Figure 1

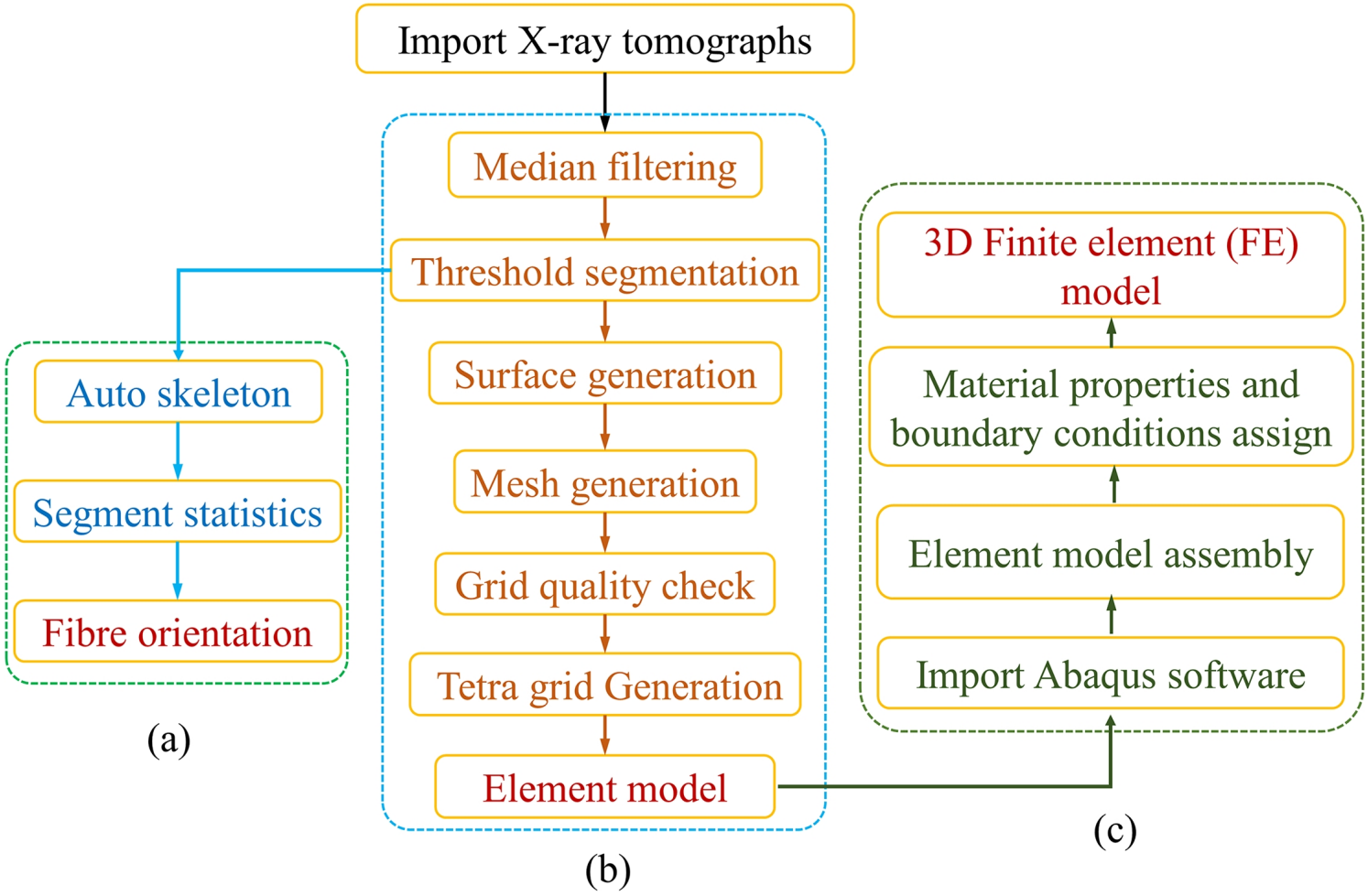
Import X-ray tomographs
Median filtering
Threshold segmentation
Surface generation
Mesh generation
Grid quality check
Tetra grid Generation
Element model
Auto skeleton
Segment statistics
Fibre orientation
(a)
(b)
3D Finite element (FE) model
Material properties and boundary conditions assign
Element model assembly
Import Abaqus software
(c)

Figure 2

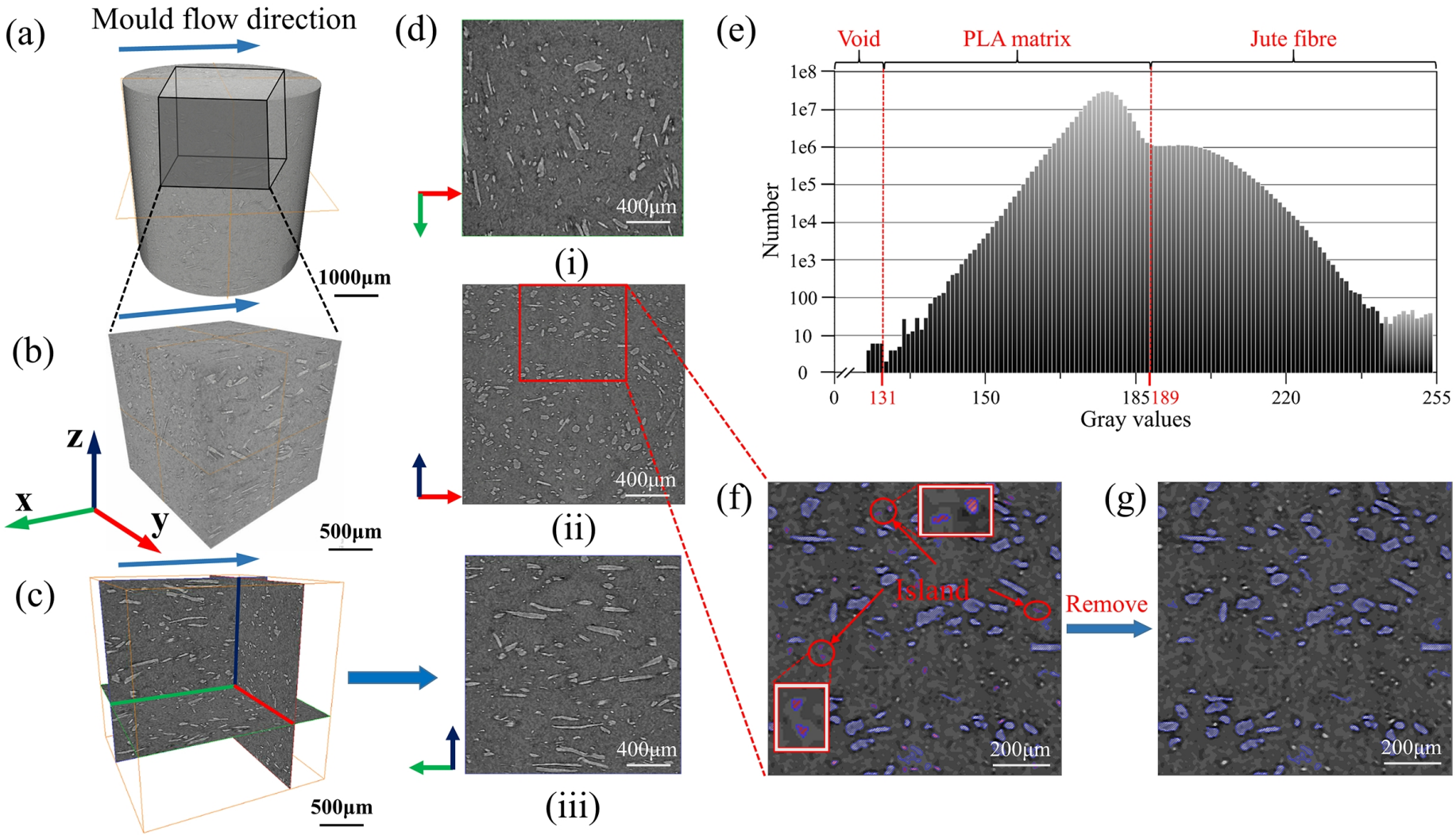
(a)
Mould flow direction
1000μm
(b)
z
x
y
500μm
(c)
500μm
(d)
400μm
(i)
400μm
(ii)
400μm
(iii)
(e)
Void
PLA matrix
Jute fibre
Number
1e8
1e7
1e6
1e5
1e4
1e3
100
10
0
0
131
150
185
189
220
255
Gray values
(f)
Island
200μm
Remove
(g)
200μm

Figure 3

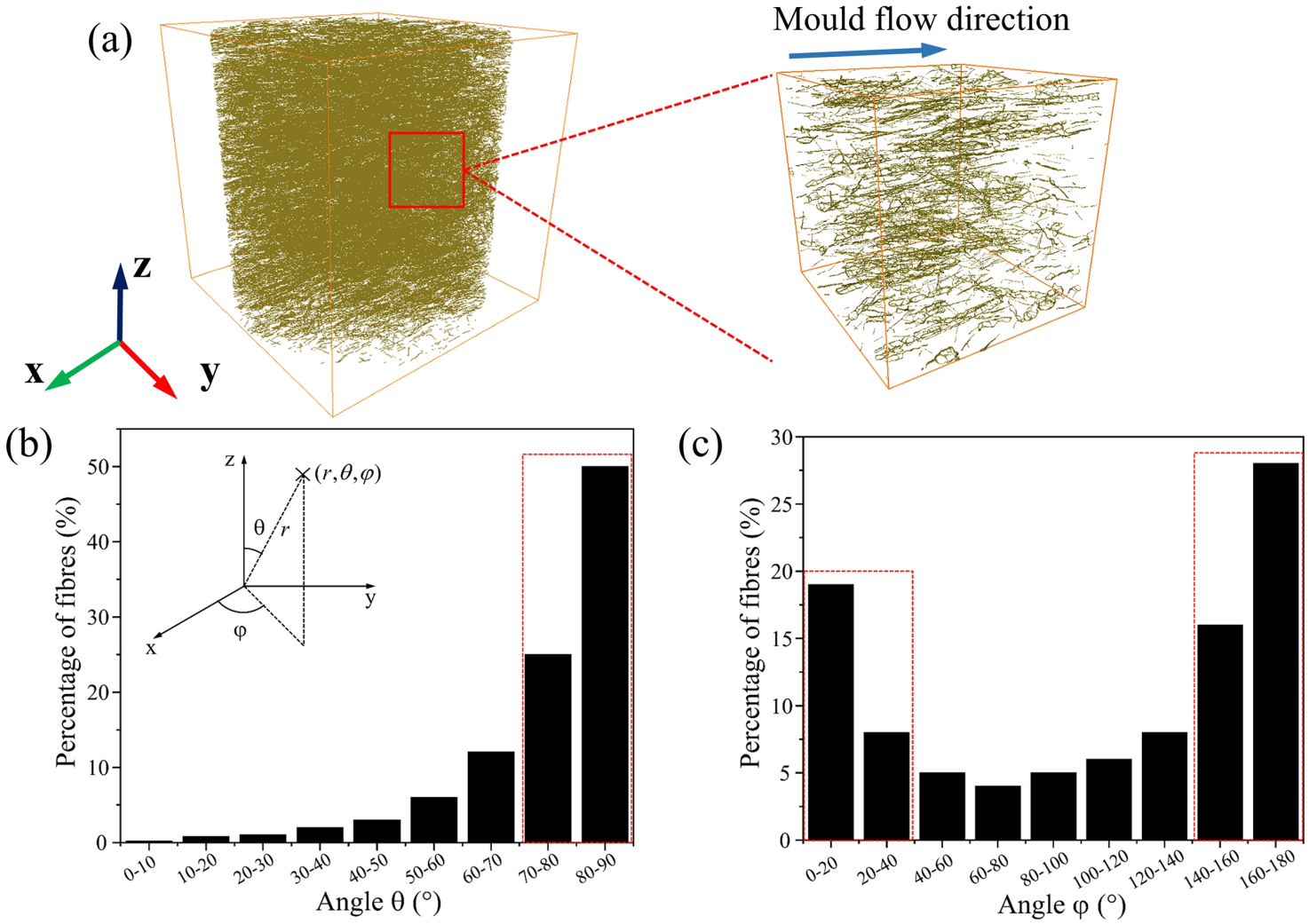
(a)
Mould flow direction
z
x
y
(b)
z
(r,θ,φ)
θ
r
y
x
φ
Percentage of fibres (%)
0
10
20
30
40
50
0-10
10-20
20-30
30-40
40-50
50-60
60-70
70-80
80-90
Angle θ (°)
(c)
Percentage of fibres (%)
0
5
10
15
20
25
30
0-20
20-40
40-60
60-80
80-100
100-120
120-140
140-160
160-180
Angle φ (°)

Figure 4

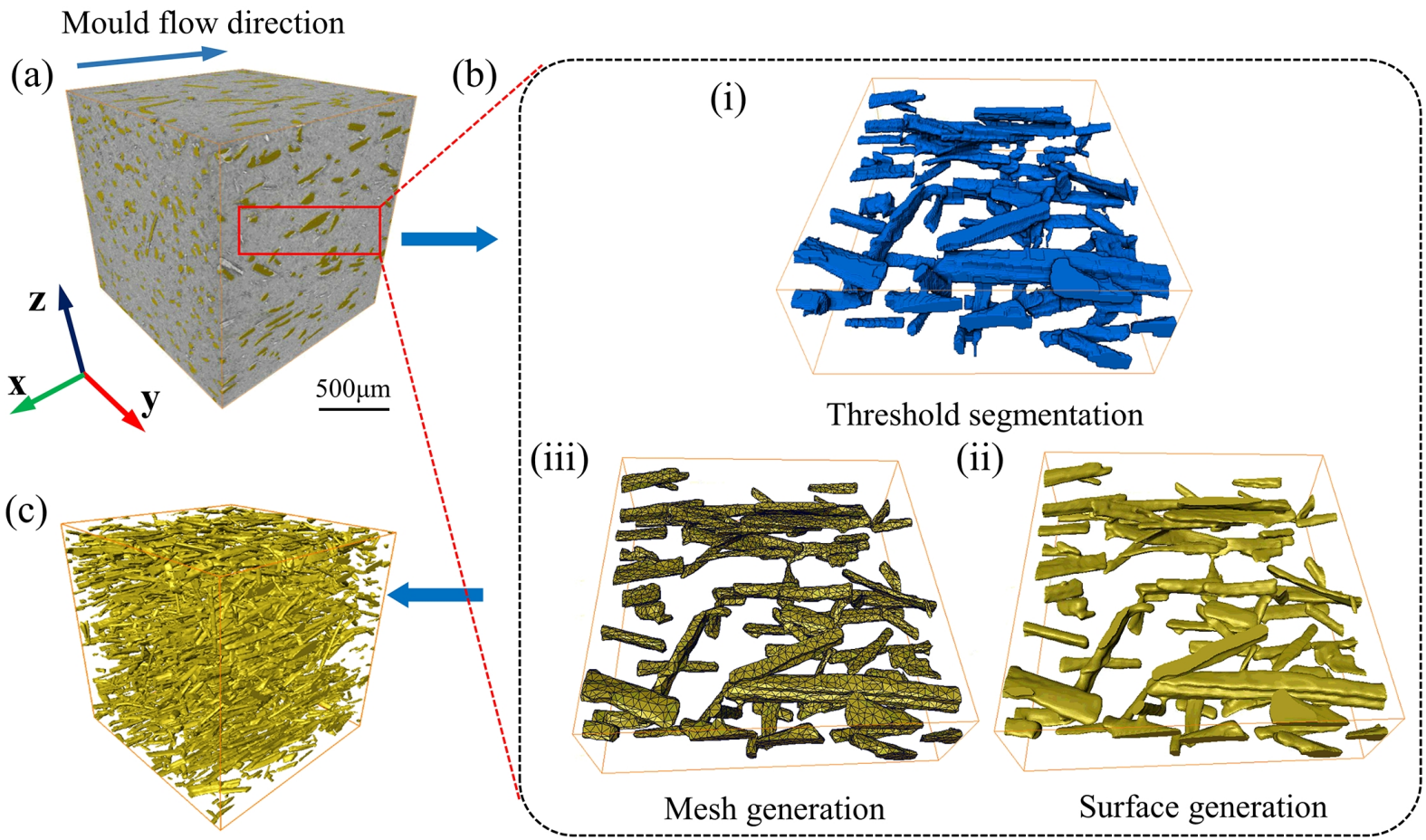
Mould flow direction
(a)
(b)
(i)
z
x
y
500μm
Threshold segmentation
(iii)
(ii)
(c)
Mesh generation
Surface generation

Figure 5

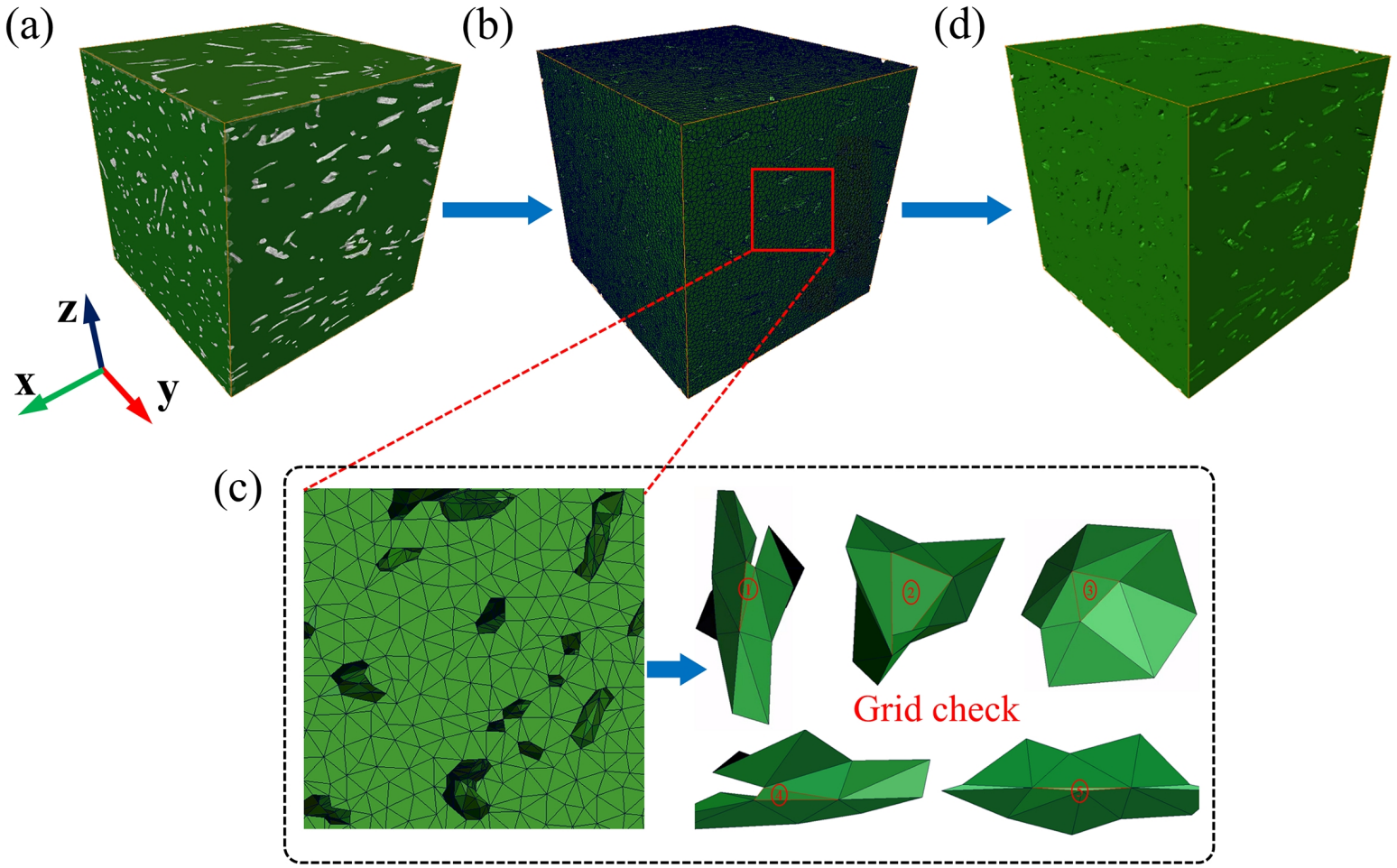

Figure 6

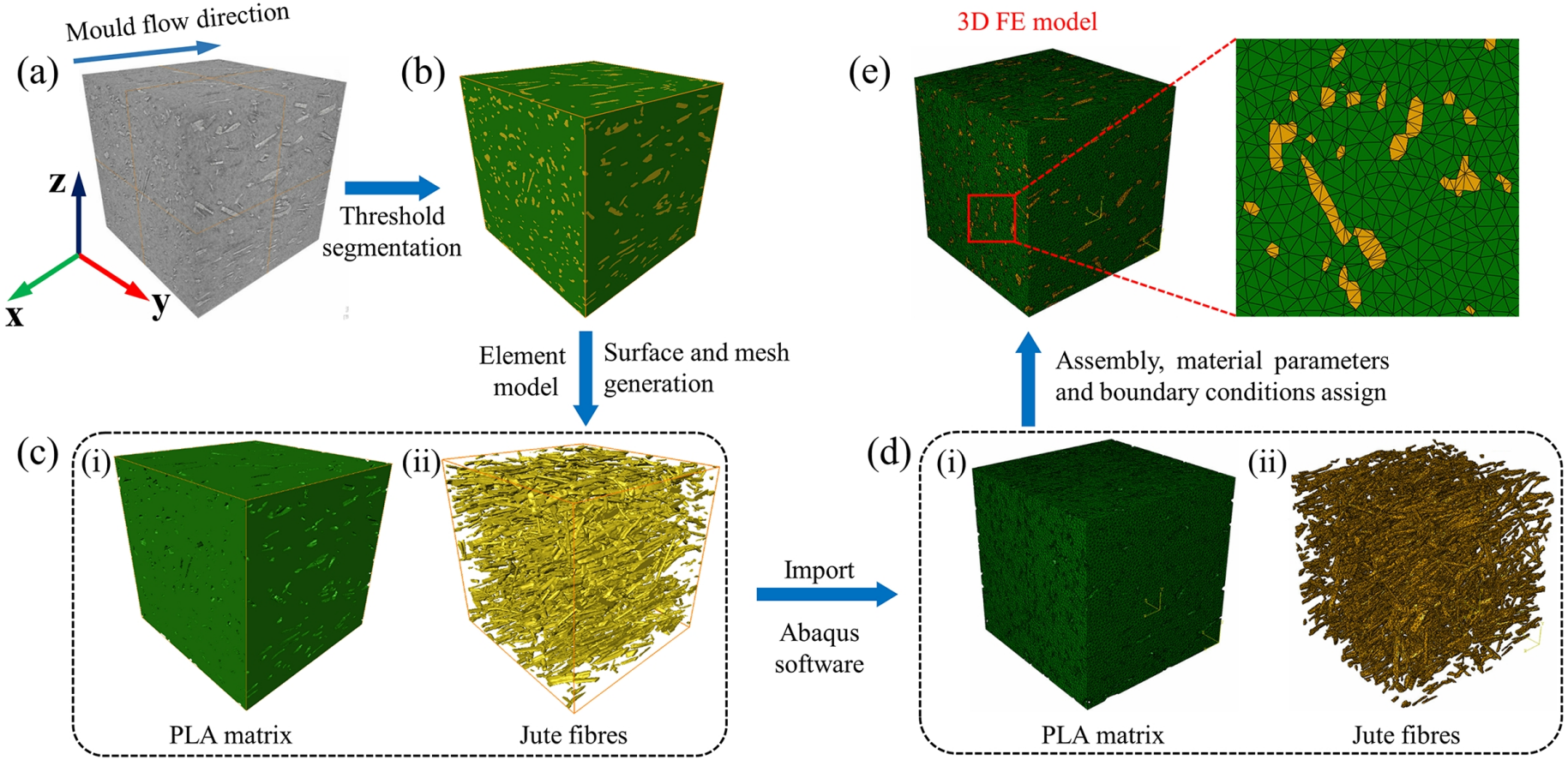
Mould flow direction
(a)
z
x
y
(b)
Threshold segmentation
Element model
Surface and mesh generation
(c)
(i)
(ii)
PLA matrix
Jute fibres
Import
Abaqus software
(d)
(i)
(ii)
PLA matrix
Jute fibres
Assembly, material parameters and boundary conditions assign
3D FE model
(e)

Figure 7

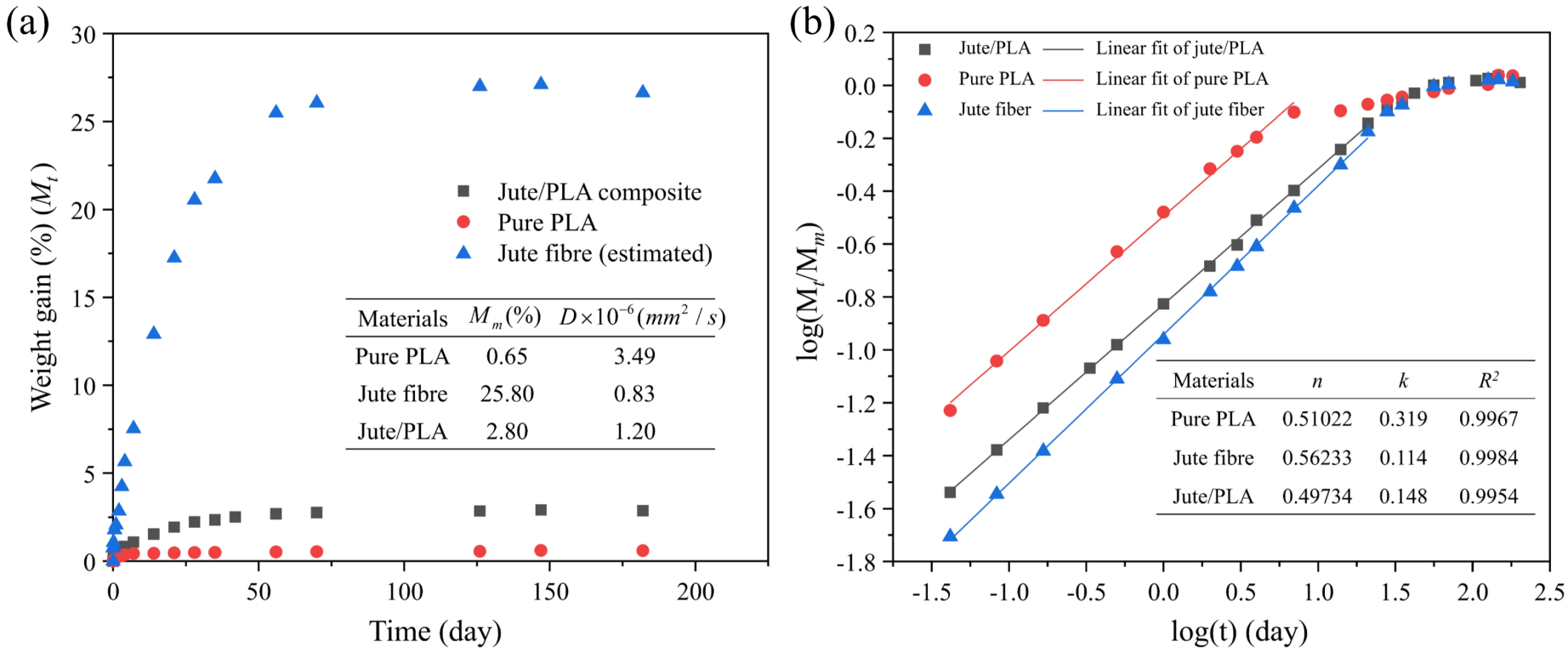
(a)
Weight gain (%) (M_t)
Time (day)
Jute/PLA composite
Pure PLA
Jute fibre (estimated)
Materials | M_m(%) | $D\times10^{-6}(mm^2/s)$
Pure PLA | 0.65 | 3.49
Jute fibre | 25.80 | 0.83
Jute/PLA | 2.80 | 1.20
(b)
log(M_t/M_m)
log(t) (day)
Jute/PLA
Pure PLA
Jute fiber
Linear fit of jute/PLA
Linear fit of pure PLA
Linear fit of jute fiber
Materials | n | k | R^2
Pure PLA | 0.51022 | 0.319 | 0.9967
Jute fibre | 0.56233 | 0.114 | 0.9984
Jute/PLA | 0.49734 | 0.148 | 0.9954

Figure 8

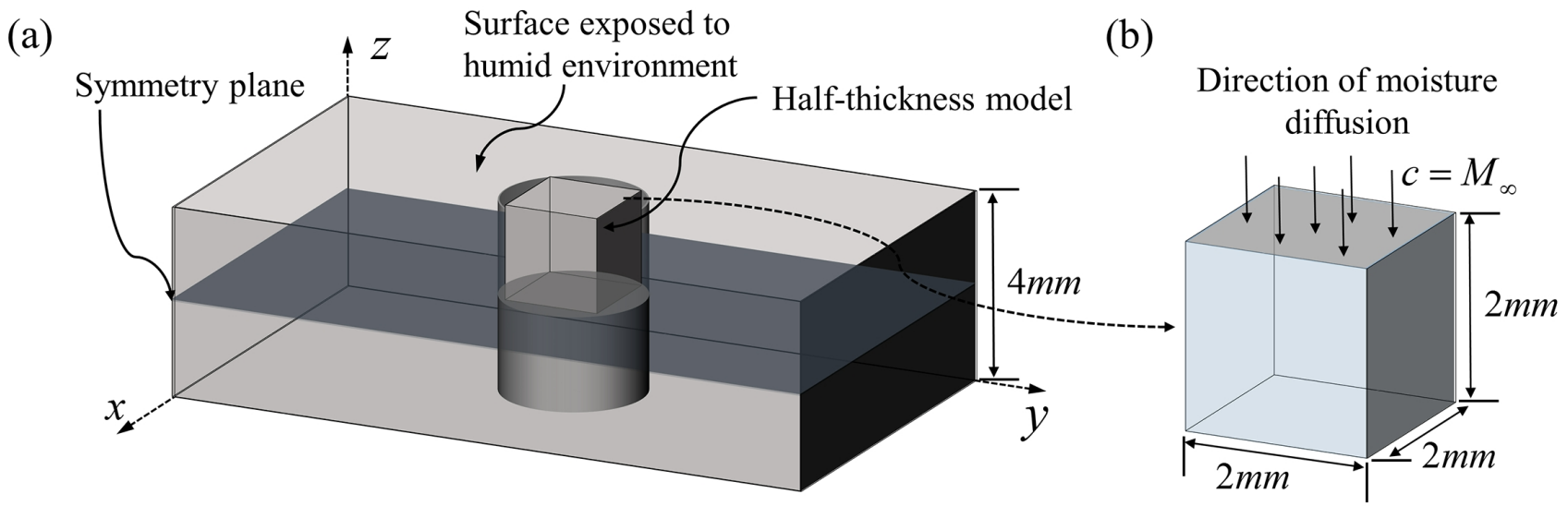

(c) Diffusion parameters of jute fibre and PLA matrix

Materials	$M_m(\%)$	$D\times10^{-6}(mm^2/s)$
PLA matrix	0.65	3.49
Jute fibre	25.80	0.83

Figure 9

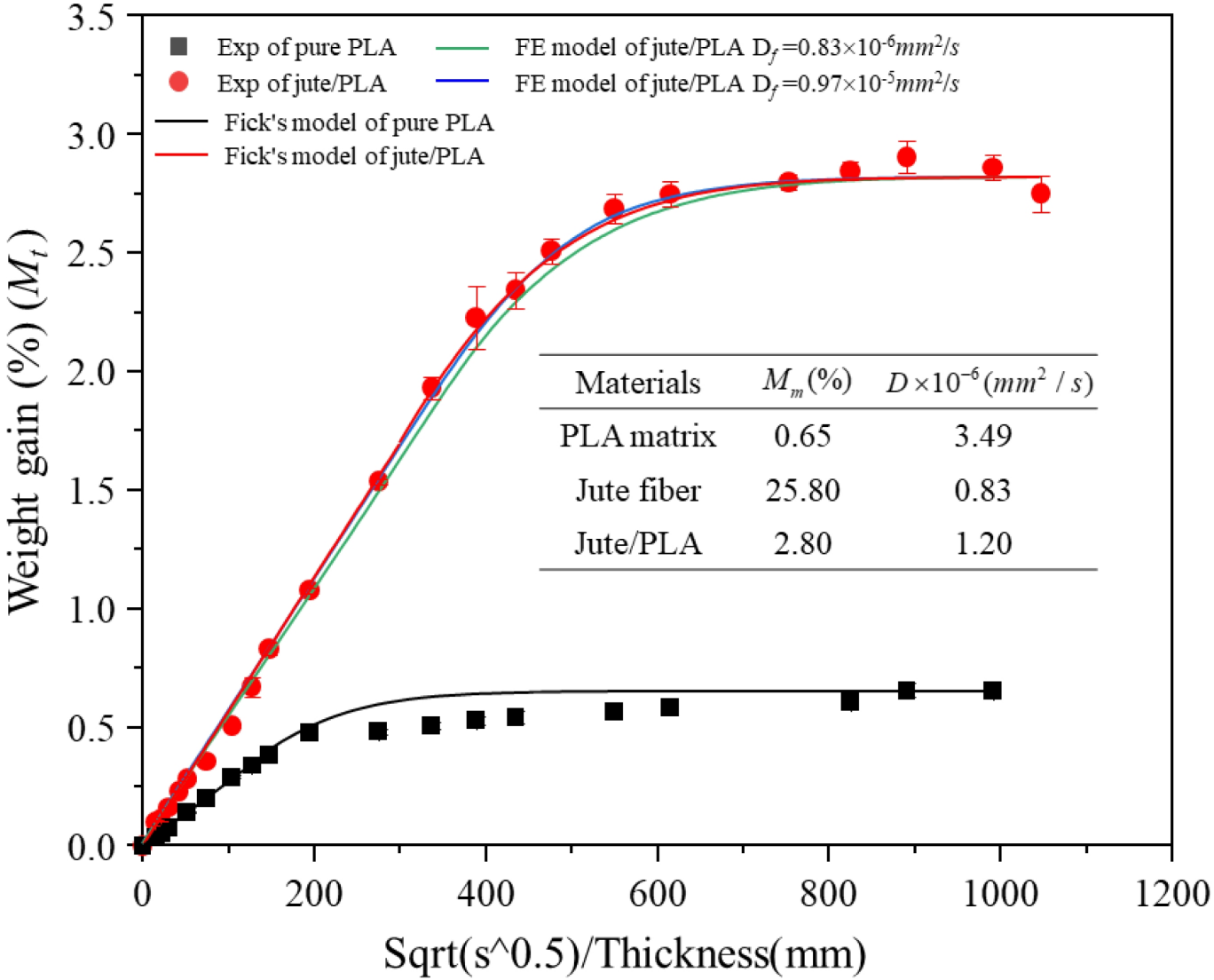

Materials	M_m(%)	$D\times10^{-6}(mm^2/s)$
PLA matrix	0.65	3.49
Jute fiber	25.80	0.83
Jute/PLA	2.80	1.20

Figure 10

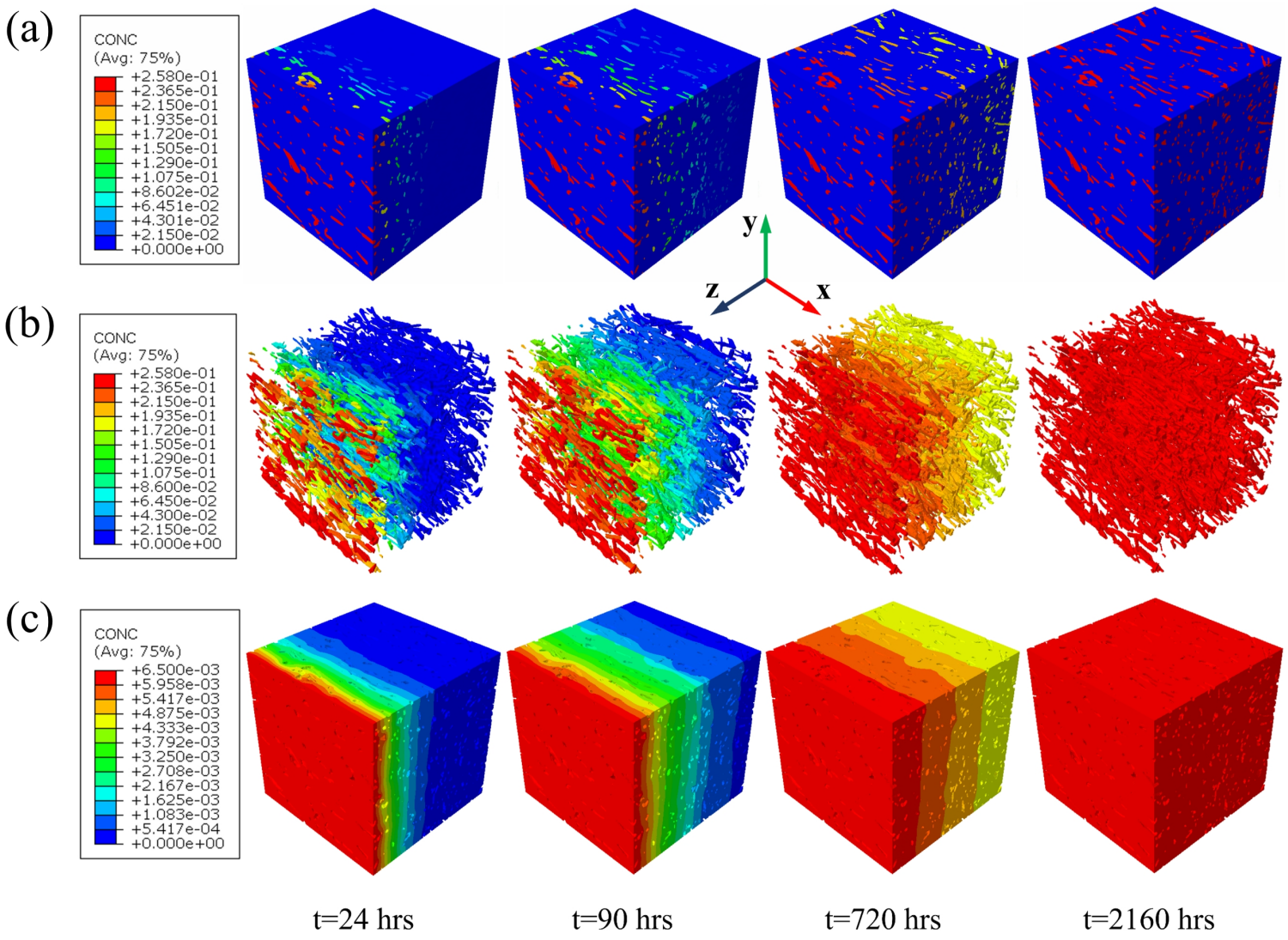
(a)
CONC
(Avg: 75%)
+2.580e-01
+2.365e-01
+2.150e-01
+1.935e-01
+1.720e-01
+1.505e-01
+1.290e-01
+1.075e-01
+8.602e-02
+6.451e-02
+4.301e-02
+2.150e-02
+0.000e+00
y
z
x
(b)
CONC
(Avg: 75%)
+2.580e-01
+2.365e-01
+2.150e-01
+1.935e-01
+1.720e-01
+1.505e-01
+1.290e-01
+1.075e-01
+8.600e-02
+6.450e-02
+4.300e-02
+2.150e-02
+0.000e+00
(c)
CONC
(Avg: 75%)
+6.500e-03
+5.958e-03
+5.417e-03
+4.875e-03
+4.333e-03
+3.792e-03
+3.250e-03
+2.708e-03
+2.167e-03
+1.625e-03
+1.083e-03
+5.417e-04
+0.000e+00
t=24 hrs
t=90 hrs
t=720 hrs
t=2160 hrs

Figure 11